Eur. Phys. J. A **22**, 519–528 (2004)
DOI 10.1140/epja/i2004-10060-6

THE EUROPEAN PHYSICAL JOURNAL A

Ice moderator experiments at very low temperatures

Comparison of experimental data with Monte Carlo simulations using new scattering law data S(α, β, T)

K. Nünighoff[1,a], Ch. Pohl[1], V. Bollini[1], A. Bubak[1], H. Conrad[1], D. Filges[1], H. Glückler[1], F. Goldenbaum[1], G. Hansen[1], B. Lensing[1], R.-D. Neef[1], N. Paul[1], D. Prasuhn[1], K. Pysz[1,3], H. Schaal[1], H. Soltner[1], H. Stelzer[1], H. Tietze-Jaensch[1], W. Bernnat[2], J. Keinert[2], M. Mattes[2], W. Ninaus[4], S. Koulikov[5], A. Smirnov[5], and M. Wohlmuther[6]

[1] Forschungszentrum Jülich GmbH, Germany
[2] Institut für Kernenergetik und Energiesysteme (IKE), Universität Stuttgart, Germany
[3] Institute of Nuclear Physics, Polish Academy of Science, Cracow, Poland
[4] Institut für Technische Physik, Technische Universität Graz, Austria
[5] Joint Institute of Nuclear Research, Dubna, Russia
[6] Paul-Scherrer Institut, Villigen, Switzerland

Received: 8 April 2004 / Revised version: 22 July 2004 /
Published online: 23 November 2004 –
Communicated by Th. Walcher

Abstract. In this article measured time-of-flight spectra and energy spectra of a water moderator operated at various temperatures between 20 K and room temperature are described. These data are used to validate generated and processed neutron scattering law data. It was possible to simulate the leakage spectrum of a water moderator at cryogenic temperatures and compare it with experimental results.

PACS. 24.10.Lx Monte Carlo simulations (including hadron and parton cascades and string breaking models) – 25.40.Fq Inelastic neutron scattering – 28.20.-v Neutron physics – 28.20.Gd Neutron transport: diffusion and moderation

1 Introduction

Water around room temperature or up to 50–60 degrees celsius is a commonly used material in research reactors and spallation neutron sources. Experiments with cryogenic water moderators at temperatures down to 20 K have already been demonstrated [1–4]. In contrast to the above-mentioned experiments, the JESSICA experiment (Jülich Experimental Spallation Target Set-up In COSY Area) allows the normalization of the measured spectra to the number of incident protons and a validation of Monte Carlo transport codes on an absolute scale. At the JESSICA experiment a water moderator at temperatures of $T = 20\,\mathrm{K}$, $T = 70\,\mathrm{K}$, and $T = 300\,\mathrm{K}$ was investigated. The measured time-of-flight and derived energy spectra were compared with Monte Carlo simulations performed with MCNPX [5], processing newly generated neutron scattering law data $S(\alpha, \beta, T)$ as well as elastic neutron scattering cross-section sets in ENDF-6 format [6]. These data take into account the molecular dynamics as well as the lattice dynamics of the moderator material to calculate the energy and momentum transfer of the incident neutrons. For the moderation of cold neutrons especially the hindered rotational modes and the translational vibrations are important. In this paper the water moderator experiments at JESSICA are described and new neutron cross-section data sets for MCNPX are presented. To validate the new cross-sections, the simulated data were compared with our experimental results and also with results of former experiments [1–4], which used a cylindrical moderator geometry and photo neutrons, but without a reflector surrounding the target and moderator.

2 Experiment

The JESSICA experiment is a full-scale mock-up of the ESS (European Spallation Source) target-moderator-reflector assembly [7] installed at the COler SYnchrotron COSY at the Forschungszentrum Jülich. Because of the low proton beam intensity, COSY is particularly suitable for studying the neutronic performance of advanced moderators, because radiolysis and activation levels are negligible. Not only can the proton beam energy be tuned from 0.8 GeV up to 2.5 GeV, the negligible activation

[a] e-mail: k.nuenighoff@fz-juelich.de

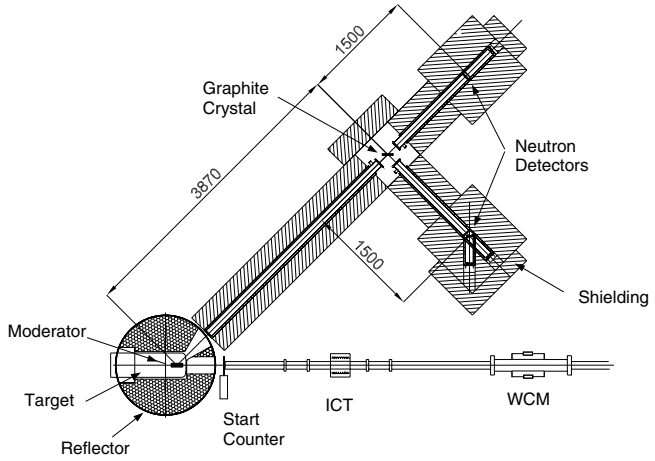

Fig. 1. Schematic drawing of the experimental set-up of the JESSICA experiment with proton beam monitors (ICT, WCM), start counter, neutron detectors, analyzer crystal, and target-moderator-reflector assembly.

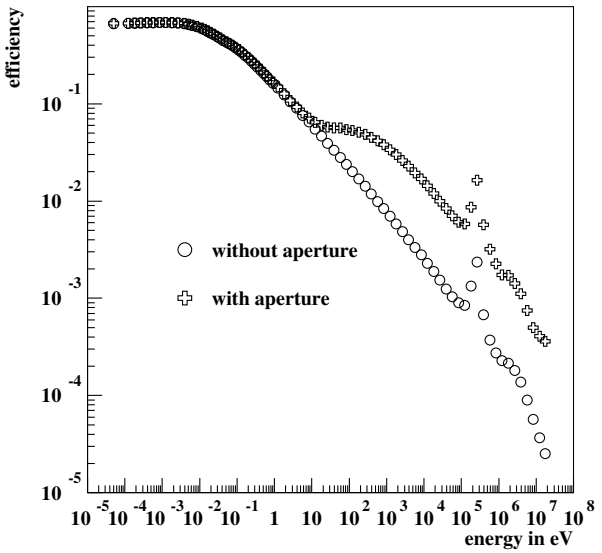

Fig. 2. Comparison of the detector efficiency with and without an aperture with an opening of $4.5\,\mathrm{cm}^3$.

rate permits one to easily modify the geometry, construction details and the materials involved. Furthermore, the neutronic performance can be studied and the gathered data can be linearly scaled to higher beam intensities as they will be available in high-power spallation neutron sources [7–10]. The experiment uses a proton beam with a kinetic energy of 1.3 GeV, a pulse length of about $0.5\,\mu$s, a repetition rate of 0.05 Hz and an intensity up to 10^9 protons per pulse. To extract such a short-pulsed beam, which was beyond the initial design of COSY, a fast kicker extraction has been developed [11]. The proton beam hits the liquid-metal target containing 35 l mercury and thereby causes a hadronic cascade which leads to the emission of neutrons. Most of the neutrons are released in the evaporation phase of the spallation reaction with a kinetic energy of 2-3 MeV. These neutrons are partly scattered back by the lead reflector with a height and a diameter of 1.3 m, respectively. The reflector consists of lead rods filling 80% of the volume. 20% of the volume was forseen for D_2O cooling, which was not necessary in our experiment due to the low beam power. Inside the reflector four moderators are positioned, two above and two below the target. This arrangement reduces the number of high-energy neutrons from leaving the target in the direction of the neutron beam lines. While three of the moderators are dummy moderators only, the bottom upstream moderator is used for the experimental investigations. This moderator can be filled with different moderator materials and can be operated at any temperature between 10 K and 300 K. All four moderators have a rectangular shape with a height of 12 cm, a width of 15 cm and a depth of 5 cm. The arrangement of the experiment with its devices is shown in fig. 1. The neutron flight path as well as the detectors are shielded in order to reduce the background which is caused by high-energy neutrons leaving the reflector and being reflected at the concrete walls of the experiment hall. These high-energy neutrons are thermalized within a 22.5 cm thick polyethylene layer (42.5 cm in case of the detector housing) surrounding the neutron flight path. The thermalized neutrons are prevented from reaching the detector by being captured inside a boric-acid layer with an average thickness of 2 cm.

2.1 Neutron time-of-flight measurement

To determine the energy spectrum of a certain moderator material, the time-of-flight spectrum is measured. A 5.37 m long neutron flight path views the moderator surface. In this case the moderator surface is perpendicular to the neutron flight path. The viewed moderator surface is limited by the cross-section of the neutron beam tube with an inner diameter $d = 10\,\mathrm{cm}$. At the end of the neutron flight path a LiGdBO scintillator [12, 13] counts the neutrons arriving at the detector. This detector has an active area of $A = 16.6\,\mathrm{cm}^2$, but to avoid deadtime effects the active area is reduced by an aperture to $A = 4.5\,\mathrm{cm}^2$. The aperture consist of a 1 mm thick cadmium layer and a 1 cm thick B_4C layer. The detector efficiency was calculated with MCNPX by simulating the neutron flux for monoenergetic neutrons impinging the detector volume and folding the obtained flux with the neutron absorption cross-section for ^{6}Li. The amount of the absorber material LiGdBO was adjusted to a measured transmission of 0.108 eV neutrons through the scintillator disk. In a further simulation the effect of the aperture was investigated. As can be seen in fig. 2, the efficiency is higher as compared to a detector without aperture for incident energies above 10 eV because the aperture becomes more and more transparent for neutrons with higher energies and thus the active detector area increases. The measurement starts when the proton beam passes through a plastic scintillator (labeled Start Counter in fig. 1) in front of the target and whenever a neutron arrives at the detector the

time of flight is measured and stored in a mulitchannel analyzer. In this way we measure the neutron time-of-flight spectrum for each single proton pulse. In order to evaluate the time-of-flight spectrum of the thermal neutrons, we performed a difference measurement. We subtracted data taken with a 1 mm thick slab of Cd in front of the flight path from the data taken without the absorber. This difference spectrum is used for the determination of the neutron temperature which is described later. Since we were also interested in the slowing-down part of the energy spectrum, we replaced the cadmium slab by a slab of boron carbide (B_4C), because the former is increasingly transparent for neutrons with energies higher than about 0.4 eV. Using Cd would therefore result in subtracting too much from the raw data.

To investigate the storage time of the thermalized neutrons within the moderator, we measured the wavelengths-dependent time-of-flight spectrum. This is done by placing a graphite monocrystal into the neutron flight path which selects specific wavelengths fulfilling the Bragg condition for the chosen Bragg angle of $\Theta = 45°$ according to

$$n \cdot \lambda = 2 \cdot d \cdot \sin\Theta. \quad (1)$$

Here λ is the wavelength in Å, d is the lattice spacing, Θ is the Bragg angle, and n is the order of the reflection. From the resulting time-of-flight spectrum we determine the pulse width at FWHM and the decay constant assuming an exponential decay of the pulse. With a lattice spacing of $d = 3.35$ Å and a Bragg angle of $\Theta = 45°$, we are able to analyze the wavelengths $\lambda = 4.74$ Å, 2.37 Å, 1.58 Å, 1.19 Å, and 0.95 Å. Higher orders cannot be resolved and vanish in the high-energy background.

2.2 Proton beam monitoring

To compare our experimental data quantitatively with Monte Carlo simulations, it is necessary to normalize the data to the number of incident protons. Due to the beam intensity of up to 10^9 protons per pulse in less than 1 μs, the resulting counting rate is too high for commonly used particle detectors like scintillators or wire chambers. We installed two beam monitors in the proton beam line as shown in fig. 1, an Integrating Current Transformer ICT [14] and a Wall Current Monitor WCM [15]. The ICT measures the current induced by the magnetic field of the proton pulse in a coil surrounding the proton beam line. This current is proportional to the number of protons in the pulse. The uncertainty of this device was measured to be better than 5% [16]. The second device measures the mirror current in the metallic beam tube and is also proportional to the number of protons per pulse.

Figure 3 illustrates the correlation between the number of protons per pulse and the number of detected neutrons per pulse. As expected, the number of protons per pulse and the number of neutrons per pulse show a linear correlation. We would like to point out that the effect of closing the neutron flight path with Cd to prevent thermal neutrons entering the neutron flight path can be seen in this correlation. As can be seen in fig. 3 in both histograms the beam intensity is very similar, but the number of neutrons per pulse is reduced by a factor of two, when the thermal neutrons are absorbed in the Cd layer.

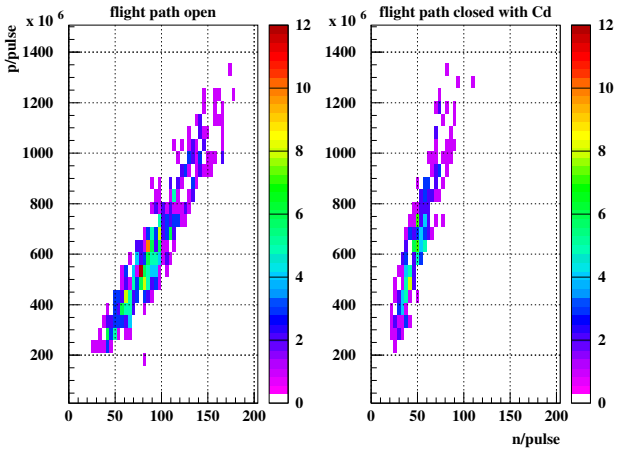

Fig. 3. Correlation between the measured number of protons per pulse and the number of detected neutrons per pulse. The histogram on the left side shows the correlation for an open neutron flight path, whereas the histogram on the right side shows the correlation in the case when the entrance to the neutron flight path is closed by a Cd layer.

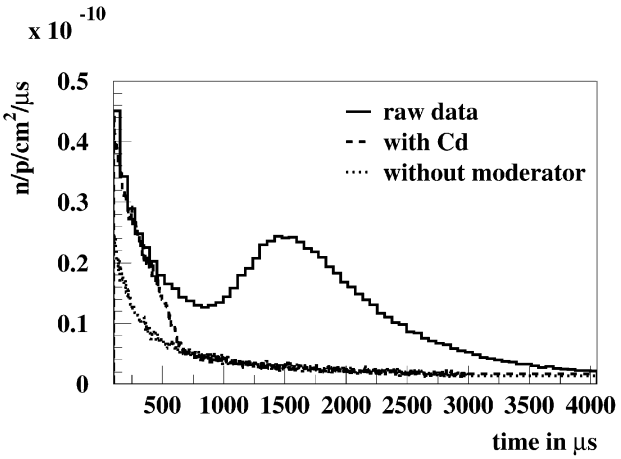

Fig. 4. Time-of-flight spectrum of a water moderator at room temperature.

3 Data analysis

3.1 Analysis of the total time-of-flight spectra

As mentioned above, the evaluation of the thermal time-of-flight spectrum is performed on the basis of a difference measurement. In fig. 4 the total time-of-flight spectrum (solid line) and the spectrum with the Cd absorber (dashed line) is plotted. Additionally, a background measurement, *i.e.* without moderator, is shown (dotted line).

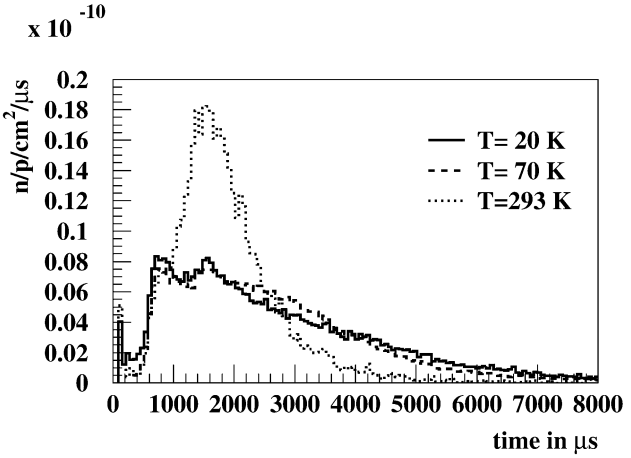

Fig. 5. Neutron time-of-flight spectra of an ice moderator at $T = 20\,\mathrm{K}$ and $T = 70\,\mathrm{K}$ compared to the time-of-flight spectrum of a water moderator at $T = 300\,\mathrm{K}$.

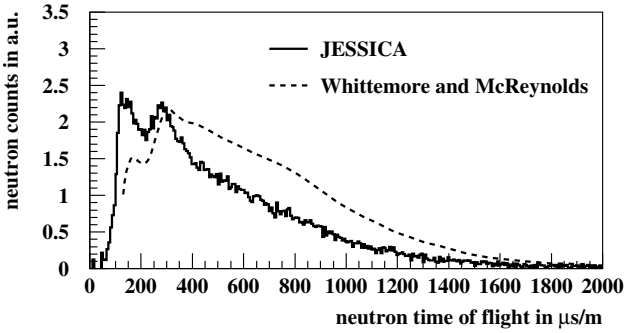

Fig. 6. Time-of-flight spectra normalized to the reciprocal velocity of the neutrons. Comparison of the spectrum of an ice moderator at $T = 20\,\mathrm{K}$ from our experiment (solid line) with the result from Whittemore and McReynolds (dashed line) [1,2] is presented.

Table 1. Neutron temperatures compared with moderator temperatures.

Moderator material	Moderator temperature	Neutron temperature
Ice	20 K	$71 \pm 4\,\mathrm{K}$
Ice	70 K	$110 \pm 2\mathrm{K}$
Water	300 K	$343 \pm 15\mathrm{K}$

It can be seen that up to $440\,\mu\mathrm{s}$ the Cd layer is transparent for all neutrons. This time corresponds to a kinetic energy of the neutron of about 0.7 eV. For lower energetic neutrons the Cd layer loses more and more of its transparency until it is a complete absorber for neutrons below 0.4 eV, *i.e.* a time of flight of about $660\,\mu\mathrm{s}$.

In fig. 5 the time-of-flight spectra for ice at $T = 20\,\mathrm{K}$ and $T = 70\,\mathrm{K}$ are compared to the spectrum of an ambient temperature water moderator. The spectra have been normalized to the number of incident protons, the active detector area, and per time bin width. Further corrections have been performed for the dead time. We would like to emphasize that these spectra are compared on an absolute scale. As expected a spectrum shift towards longer flight times —*i.e.* lower kinetic energy of the neutrons— is observed for lower moderator temperatures. The small peak at about $800\,\mu\mathrm{s}$ is an effect caused by the decreasing absorption cross-section of the cadmium layer. In this region Cd is partially transparent for thermal and epi-thermal neutrons but the peak is independent of the moderator material and moderator temperature.

By normalizing the time of flight to the length of the neutron flight path, *i.e.* normalized to the reciprocal velocity, we are able to compare our data with those by Whittemore and McReynolds [1,2] (see fig. 6). In contrast to our experiment Whittemore and McReynolds used a cylindrical moderator with a re-entrant hole. They measured the neutron current which left the moderator through the re-entrant hole as well as through the opposite surface. The latter spectrum was used to compare it with our spectrum. As can be seen in fig. 6 the maximum lies at the same position at about $300\,\mu\mathrm{s/m}$. However, the shape of both spectra differ, especially the change of the slope at $800\,\mu\mathrm{s/m}$ cannot be clearly seen in our experiment. One reason for the differences of both spectra could be the different moderator geometries.

Assuming a Maxwellian distribution of the velocity of the neutrons, we are able to determine the neutron temperature. Transforming the time-dependent flux $\Phi(t)$ into the velocity-dependent flux $\Phi(v)$, the neutron temperature can be determined by the slope of the straight line in a semi-logarithmic plot based on eq. (2):

$$\ln\left(\frac{\Phi(v)}{v^3}\right) = \ln\left(\frac{2\cdot\Phi_0}{v_T^4}\right) - \frac{m_\mathrm{n}}{2\cdot k_\mathrm{B}\cdot T}\cdot v^2. \qquad (2)$$

In eq. (2) v denotes the velocity of the neutrons, m_n the neutron mass, k_B the Boltzmann constant, v_T velocity of the neutron at temperature T, and T the neutron temperature. The neutron temperatures obtained from eq. (2) for two ice moderators and an ambient temperature water moderator are listed in table 1 and compared with the real moderator temperatures. The neutron temperatures are higher than the moderator temperatures. The reason for this discrepancy is that the neutron distribution has a slowing-down source of epithermal neutrons and a loss of $1/v$ absorption compared to the moderator molecular energy distribution. In balance this results in a hardened Maxwell-Boltzmann distribution of the neutrons, if the absorption is not too strong and has no resonance structure.

In the next step we determine the energy spectra from the time-of-flight spectra by transforming $\Phi(t)$ into $\Phi(E)$ [17]. In this case we perform the data analysis in the same two steps as mentioned for the analysis of the time-of-flight spectra, but using B_4C instead of Cd in order to observe the expected $1/E$ slope in the moderator spectrum. The resulting energy spectra for ice and water are plotted in fig. 7. The shift of the maximum towards lower energies for lower moderator temperatures can be seen. The maximum for the water moderator lies at an energy of

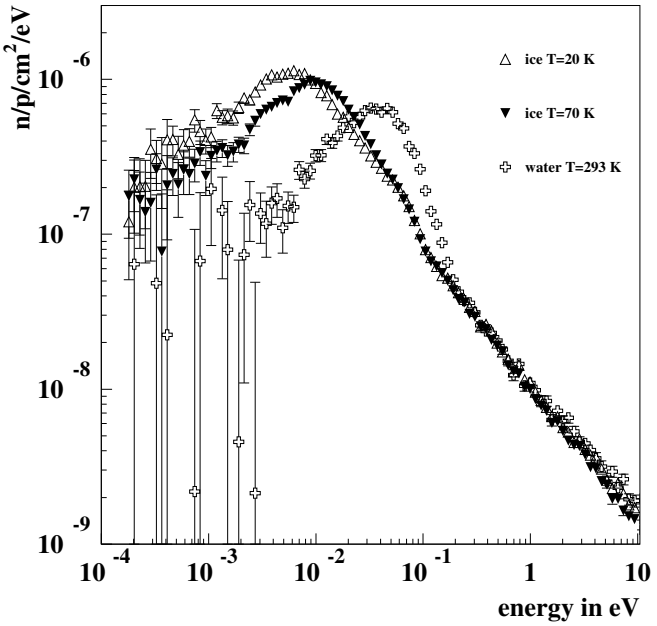

Fig. 7. Energy spectra of an ice moderator at $T = 20\,\mathrm{K}$ and $T = 70\,\mathrm{K}$ compared to the energy spectrum of a water moderator at $T = 300\,\mathrm{K}$.

40 meV, for an ice moderator at $T = 70\,\mathrm{K}$ at 10 meV, and for the ice moderator at $T = 20\,\mathrm{K}$ at 6 meV. The plotted data are normalized to the number of incident protons, the active detector area, the energy bin width, and the detector efficiency. Comparing the energies of the maxima obtained at JESSICA with those of Inoue *et al.* [3, 4] a slight shift of the JESSICA data can be seen. This shift is due to the fact that Inoue *et al.* measured the energy spectra emitted from a re-entrant hole and therefore probed the flux inside the moderator rather than the leakage flux on the surface.

3.2 Wavelength-dependent time-of-flight spectra

A more detailed view on the time behavior of the neutron pulses can be obtained by measuring the wavelength-dependent time-of-flight spectra. The technique is described in sect. 2.1. In fig. 8 the wavelength-dependent time-of-flight spectra for water at $T = 300\,\mathrm{K}$ and ice at $T = 20\,\mathrm{K}$ are plotted. The shift of the spectrum towards lower kinetic energies, *i.e.* longer flight times, for lower moderator temperatures can also be seen in fig. 8. Whereas the intensity for water at $\lambda = 1.19\,\text{Å}$ is higher than for ice, the exact opposite is true for $\lambda = 2.37\,\text{Å}$ or $\lambda = 4.74\,\text{Å}$. At longer wavelengths the colder moderator shows more intensity. The pulse widths (FWHM) and decay constants for the two temperatures have been evaluated at wavelengths of 1.19 Å, 1.58 Å, and 2.36 Å. The data are given in table 2. These data are important for the design of new neutron scattering instruments at spallation neutron sources and are listed in table 2. It can be seen that the cold ice moderator reduces the pulse width

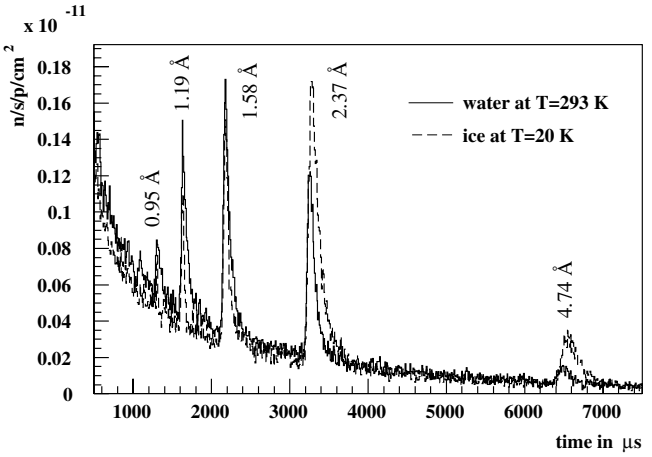

Fig. 8. Wavelength-dependent time-of-flight spectra of an ice moderator at $T = 20\,\mathrm{K}$ (dotted line) and of a water moderator at $T = 300\,\mathrm{K}$ (solid line).

Table 2. Pulse width and decay time for several wavelengths for a water moderator at room temperature and ice at 20 K.

	1.19 Å	1.58 Å	2.37 Å
300 K			
pulse width FWHM in μs	58.7	92.1	96.9
decay constant in $\mu\mathrm{s}^{-1}$	0.016	0.014	0.015
20 K			
pulse width FWHM in μs	36	56	101
decay constant in $\mu\mathrm{s}^{-1}$	0.057	0.039	0.019

by about 39% for wavelengths of 1.19 Å and 1.58 Å, and agrees within 4% for 2.37 Å compared to an ambient temperature water moderator. Furthermore the decay constant is higher in the case of an ice moderator than in a water moderator at 300 K resulting in a faster decay of the pulse. This will allow a higher time resolution in a real neutron spallation source.

4 Comparison with Monte Carlo simulations

To perform Monte Carlo simulations of cold moderator materials MCNPX scattering kernels derived from scattering law data are mandatory. To evaluate new $S(\alpha, \beta, T)$ data sets the crystalline structure and its dynamics of the material needs to be known. The latter can be obtained from several experiments [18–21] using incoherent inelastic neutron scattering. The data showed that ice at these temperatures and under normal pressure has a hexagonal closed-packed lattice structure. To generate the new data the model of Nakahara [22] was chosen in order to describe the frequency distribution in the range of the acoustic vibrational modes of ice with a hexagonal closed-packed lattice structure known as ice Ih. The frequency band of the hindered rotational modes was approximated by a Gaussian distribution (see fig. 9). The optical oscillations of the streching vibrations are considered as discrete Einstein

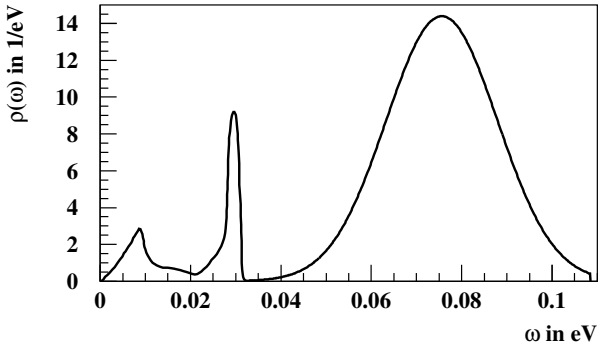

Fig. 9. Continuous part of the frequency distribution of H bound in ice Ih.

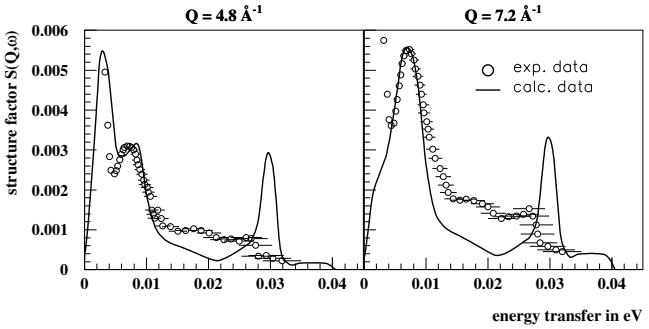

Fig. 10. Dynamical structure factor of light water ice at $T = 2\,\mathrm{K}$. Comparison between inelastic neutron scattering measurements [21] and calculated data using IKE scattering law data [23] is presented.

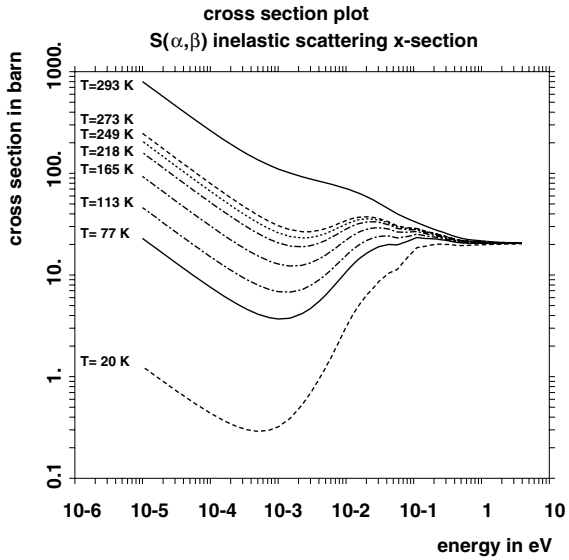

Fig. 11. MCNPX neutron cross-sections for ice (inelastic) for several temperatures and water at $T = 293.6\,\mathrm{K}$ (elastic and inelastic).

δ-oscillators [23]. This frequency distribution was used to generate $S(\alpha, \beta, T)$ data and additionally elastic neutron scattering cross-sections in ENDF-6 [6] format with the code LEAPR of the NJOY code system [24]. As a validation especially of the inelastic neutron scattering data in

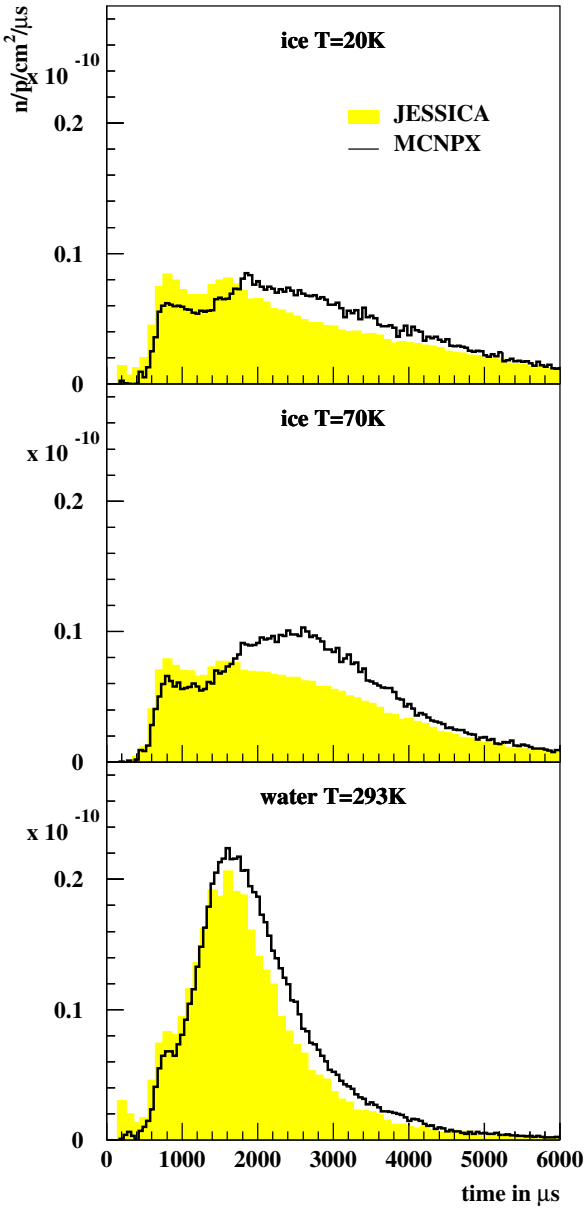

Fig. 12. Comparison of the time-of-flight spectra between JESSICA and MCNPX for an ice moderator operated at 20 K and 70 K and a water moderator at room temperature. The shaded area represents the experimental data and the solid line the MCNPX simulation.

fig. 10 a comparison is presented between an incoherent inelastic neutron scattering measurement carried out at the Jülich research reactor [21] of the dynamical structure factor $S(Q, \omega)$ of light water ice at $T = 2\,\mathrm{K}$ and the IKE data. An excellent agreement of the peak structure resulting from the translational vibrations in ice Ih can be seen. These data in ENDF-6 format were further processed with ACER of NJOY to generate data sets applicable for MCNPX. In fig. 11 the neutron cross-sections for water at $T = 293.6\,\mathrm{K}$ (elastic and inelastic) and ice for several temperatures between $T = 20\,\mathrm{K}$ and water at $T = 293.6\,\mathrm{K}$

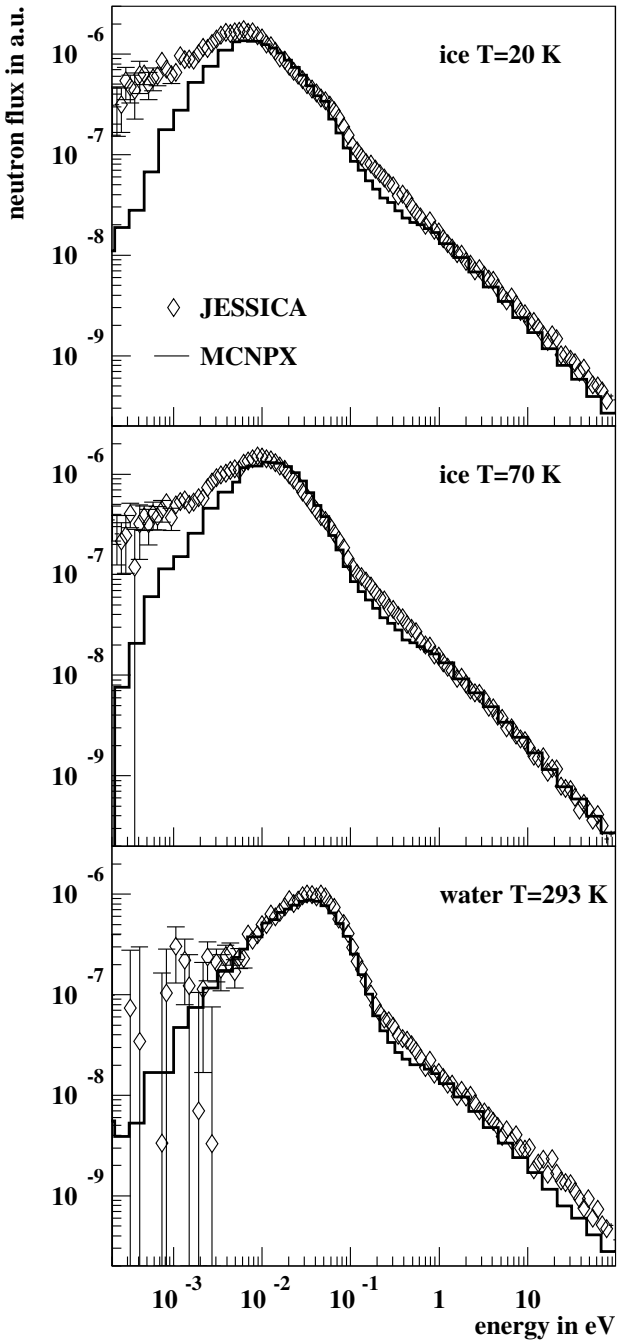

Fig. 13. Comparison of the energy spectra between JESSICA (open diamonds) and MCNPX (solid line) for an ice moderator operated at 20 K and 70 K and a water moderator at room temperature. The experimental data are normalised to the value at 1 eV of the simulated spectra.

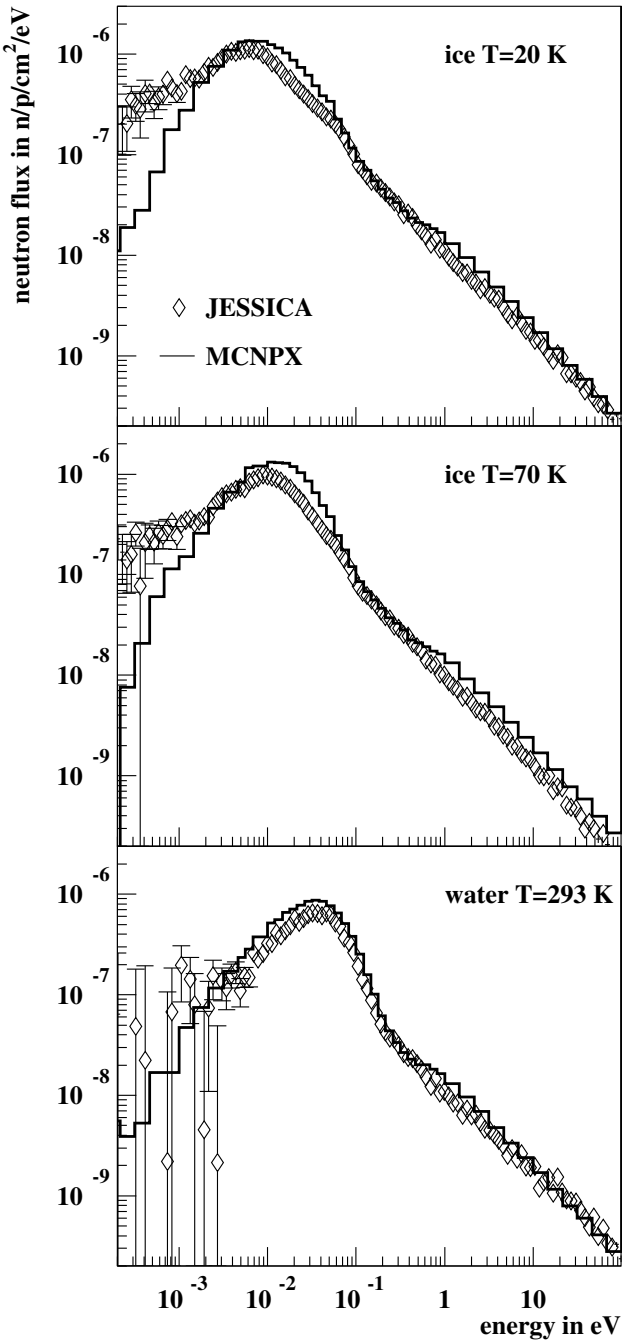

Fig. 14. Same as fig. 13, but compared on an absolute scale.

(only inelastic) are plotted. These cross-sections were used to simulate the JESSICA experiment. Additionally, the data were validated on measurements performed by Inoue *et al.* [3,4]. First, the time-of-flight spectra of a water moderator and an ice moderator measured at the JESSICA experiment are compared with MCNPX simulations. The data are normalized to the number of incident protons, to the detector area in cm^2, and to the bin width in μs. The detector efficiency is included in the simulated spectra.

Figure 12 shows that the simulated data are not in perfect agreement with the experimental data. Whereas the spectra are in accordance for flight times shorter than 1400 μs —corresponding to an energy regime where in the simulation no special $S(\alpha, \beta)$ treatment is performed— the MCNPX simulations lead to results which are greater than the experimental data by 42%, 54%, and 32% for ice at 20 K, ice at 70 K, and water at 293 K, respectively. For

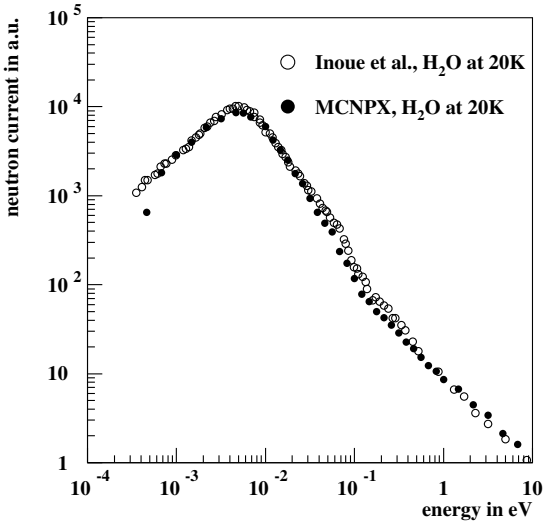

Fig. 15. Comparison of the energy spectra of an ice moderator measured by Inoue *et al.* (open circles) [3,4] and simulated with MCNPX (solid circles) at $T = 20\,\mathrm{K}$.

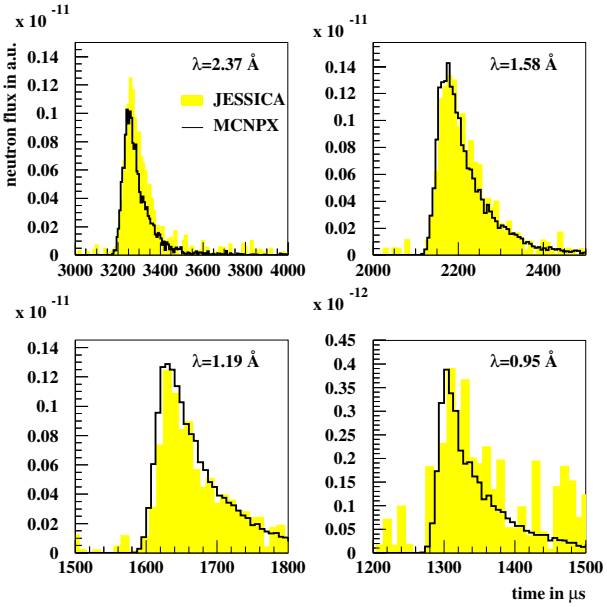

Fig. 16. Comparison of measured and simulated time-of-flight spectra for different wavelengths λ of a water moderator at room temperature.

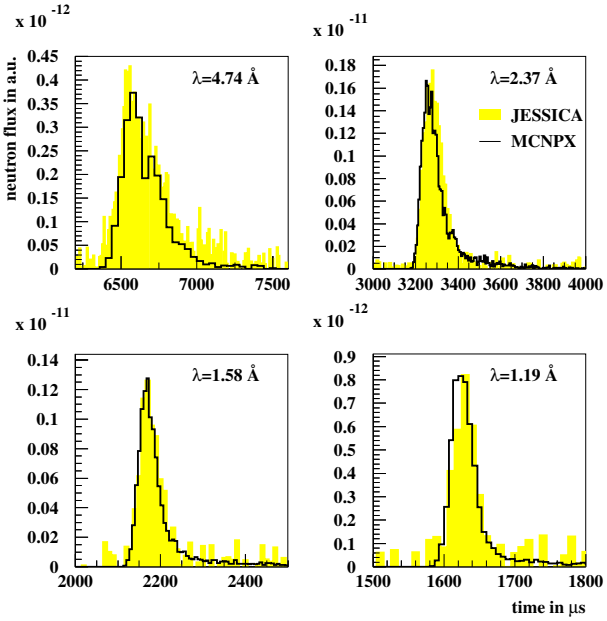

Fig. 17. Comparison of measured and simulated time-of-flight spectra for different wavelengths λ of an ice moderator operated at $T = 20\,\mathrm{K}$.

the MCNPX simulations the geometry of the experiment was modeled and a point detector with the same distance to the moderator surface as in the experiment was applied. In contrast to the experiment with a Monte Carlo simulation, we are able to determine the energy spectra directly. The obtained energy spectra are shown in fig. 13 and compared with the energy spectra derived from experimental data.

In this figure the measured data are normalised in such a way that the experimental and simulated data match at 1 eV. It can be seen that the shape of the measured neutron energy spectrum in the water moderator is in good agreement with the Monte Carlo simulations. For the neutron spectra in the ice moderator at 20 K and 70 K the agreement below 10 meV is not so good. The maximum of the calculated leakage spectra of the 20 K ice moderator is harder by about 1 meV and by about 10 meV for the 70 K ice moderator. Furthermore the Monte Carlo simulations underestimate the measured spectra in the energy range from 20 meV to 100 meV.

With the proton beam monitors the number of incident protons per pulse can be determined and we are able to normalize our neutron time-of-flight spectra to these numbers. Figure 14 shows the same as fig. 13, but on an absolute scale. The neutron fluxes from the Monte Carlo simulations show 60% higher values than the experimental data in the vicinity of the respective maxima.

In addition to the JESSICA experiment also the experiment from Inoue *et al.* [3, 4] was simulated with the new cross-section data. Instead of simulating the photo-neutron generation due to an incident electron beam hitting a tungsten target, an evaporation spectrum — showing a similar energy distribution as the spectrum of photo-neutrons— was used as a source in the Monte Carlo simulation. The simulated energy spectra are compared with the experimental data of those neutrons leaving the moderator through a re-entrant hole according to the experimental set up of Inoue *et al.* [3,4]. In fig. 15 the experimental data are plotted *versus* the result of the simulation. Both spectra are in very good agreement, except for the energy range of 30–300 meV, where the MCNPX simulation slightly underestimates —same as for the JESSICA experiment— the experimental spectrum by up to 20%. The maximum of the spectrum is at about 5 meV. This is

Table 3. Comparison of the FWHM of the experimentally measured peaks and MCNPX simulations for different wavelengths λ for ice at $T = 20\,\mathrm{K}$ and water at $T = 293\,\mathrm{K}$.

Wavelength λ	JESSICA	MCNPX
ice $T = 20\,\mathrm{K}$		
1.19 Å	$36\,\mu\mathrm{s}$	$40 \pm 14\,\mu\mathrm{s}$
1.58 Å	$56\,\mu\mathrm{s}$	$46.2 \pm 14\,\mu\mathrm{s}$
2.37 Å	$101\,\mu\mathrm{s}$	$86.7 \pm 14\,\mu\mathrm{s}$
4.74 Å	$286\,\mu\mathrm{s}$	$280 \pm 60\,\mu\mathrm{s}$
water $T = 293\,\mathrm{K}$		
1.19 Å	$58.7\,\mu\mathrm{s}$	$59.2 \pm 14\,\mu\mathrm{s}$
1.58 Å	$92.1\,\mu\mathrm{s}$	$73.4 \pm 14\,\mu\mathrm{s}$
2.37 Å	$96.9\,\mu\mathrm{s}$	$87.4 \pm 14\,\mu\mathrm{s}$

1-2 meV lower than compared with the results from JESSICA and is due to the fact that Inoue *et al.* measured the energy spectra inside the moderator vessel by looking through a re-entrant hole inside the moderator, whereas our spectrum was measured by viewing the moderator surface.

Not only the total time-of-flight spectra and energy spectra have been compared with Monte Carlo simulations, but also the wavelength-dependent time-of-flight spectra were simulated. Since MCNPX is not able to simulate the neutron scattering dependent on the crystal lattice, another technique was applied. For each wavelength λ the crystal reflects a certain wavelength band out of the primary neutron beam. This wavelength band was splitted into eleven energy groups, five below and five above the desired wavelength. The time-of-flight spectrum was silmulated taken only these eleven energy groups into account. The neutron flux in each energy bin was weighted with a Gaussian distribution. The mean value is the energy of the wavelength to be studied and the width of the wavelength band was assumed to be 2σ. However, a comparison on an absolute scale is not possible and the spectra shown in figs. 16 and 17 are normalized to the peak value of the experimental data. As can be seen in figs. 16 and 17 the agreement between the simulated wavelength-dependent time-of-flight spectra and the experimental ones is very good. Only for the water moderator for $\lambda = 0.95$ Å larger deviation could be observed, which is due to the insufficient statistics at this high order of the Bragg reflection. In table 3 the determined peak widths as FWHM are listed. Here also the agreement between the JESSICA experiment and the MCNPX simulation can be seen.

5 Conclusion

With the JESSICA experiment time-of-flight spectra and energy spectra for a water and an ice moderator at different temperatures were measured on an absolute scale, *i.e.* neutrons reaching the detector per incident proton. The dependence on the temperature was seen in the time-of-flight spectra as well as in the energy spectra. The neutron temperatures deduced from the time-of-flight measurements were as expected. For the first time Monte Carlo simulations with MCNPX of an ice moderator have been performed and have been compared with experimental data on an absolute scale. It can be observed that the spectrum inside the moderator can be described very well, but the surface leakage spectrum is not in perfect agreement with the experimental data. From physical aspects interpreting the neutron scattering dynamics in ice this is not understood because differential and integral calculated neutron cross-sections compared with experiments agree very well, although the assumed frequency distribution is handled as usual in harmonic approximation.

This work is partly supported by the TMR program of the European Community under contract No.: FMRX-CT98-0244. The JESSICA Collaboration would like to thank the technical staff from the COSY accelerator for providing the short-pulsed proton beam.

References

1. W.L. Whittemore, A.W. McReynolds, *Differential Neutron Thermalization*, Annual Summary Report, GA-2503, (General Atomic, San Diego, 1961).
2. A.W. McReynolds, W.L. Whittemore, *Inelastic Scattering of Neutrons from Very Cold Materials*, S33-35 (IAEA, 1962) p. 421.
3. K. Inoue, N. Otomoe, J. Nucl. Sci. Technol. **13**, 389 (1976).
4. K. Inoue *et al.*, At. Energy Soc. J. **21**, 865 (1979).
5. H.G. Hughes *et al.*, *MCNPX–The LAHET/MCNP Code Merger*, X-Division Research Note XTM-RN(U)97-012, LA-UR-97-4891, Los Alamos National Laboratory (1997).
6. V. McLane (Editor), ENDF-102, Data Formats and Procedures for the Evaluated Nuclear Data File, ENDF-6, BNL-NCS 44945-01/04-Rev.
7. *The European Spallation Source Project*, Vol. **III**, report ESS-96-53-M, ISBN 090 237 6659, 1996.
8. *The European Source Project*, Vol. **III**, Technical Report, ISBN 3-89336-303-3, 2002.
9. *National Spallation Neutron Source. Executive Summary*, Oak Ridge National Laboratory, May 1997.
10. *High-Intensity Proton Accelerator Facility Project, J-PARC*, `http://j-parc.jp`.
11. J. Dietrich *et al.*, *Proceedings of the European Particle Accelerator Conference 2004, Vienna, Austria*, `http://epac.web.cern.ch`.
12. J.B. Czirr *et al.*, Nucl. Instrum. Methods A **424**, 15 (1999).
13. J.B. Czirr *et al.*, Nucl. Instrum. Methods A **476**, 309 (2002).
14. BERGOZ Instrumentation, Saint Genis Pouilly, France.
15. H. Lawin *et al.*, *IKP Annual Report 1991*, Forschungszentrum Jülich, report JÜL-2590(1991), ISSN 0366-0885.
16. J.-P. Revol, *The TARC Experiment (PS211): Neutron Driven Transmutation By Adiabatic Reonance Crossing*, CERN 99-11, ISSN 0007-8328, 1999.
17. Ch. Pohl, PhD Thesis, *Berichte des Forschungszentrum Jülich JÜL-4071*, Forschungszentrum Jülich, ISSN 0944-2952, 2003.
18. J.C. Li *et al.*, Physica B **156** & **157**, 376 (1998).

19. D.D. Klug *et al.*, Phys. Rev. **44**, 841 (1991).
20. H. Fukazawa, S. Ikeda, S. Mae, Chem. Phys. Lett. **282**, 215 (1998).
21. H. Conrad *et al.*, *Proceedings of the 16th Meeting of the International Collaboration on Advanced Neutron Sources*, ISSN 1433-559X, 2003.
22. Y. Nakahara, J. Nucl. Sci. Technol. **5**, 635 (1968).
23. J. Keinert, M. Mattes, W. Bernnat, *Thermal neutron cross section data for light water ice, liquid hydrogen and solid methane for the temperature range from 14 K up to 273 K in MCNP(X) format*, IKE 6-198, Universität Stuttgart, 2002.
24. R.E. MacFarlane, C.L. Muir, The NJOY Nuclear Data Processing System Version 91, LA-12740, Los Alamos National Laboratory (1994).